# High-Performance Microring-Assisted Space-and- Wavelength Selective Switch

**Conference Paper** · January 2020

DOI: 10.1364/OFC.2020.Th2A.7



**4 authors**, including:

Qixiang Cheng
University of Cambridge
**83** PUBLICATIONS **719** CITATIONS
SEE PROFILE

Keren Bergman
Columbia University
**592** PUBLICATIONS **10,058** CITATIONS
SEE PROFILE

# High-Performance Microring-Assisted Space-and-Wavelength Selective Switch

**Yishen Huang*, Qixiang Cheng, Anthony Rizzo, Keren Bergman**
*Department of Electrical Engineering, Columbia University, New York, NY, 10027, USA*
*y.huang@columbia.edu*

**Abstract:** We introduce a novel design of space-and-wavelength selective switch using microring-assisted Mach-Zehnder interferometers. A 2×2×2λ elementary switch block is demonstrated with full spatial and wavelength switching capabilities, showing 20dB crosstalk suppression and 19dB extinction ratio.
**OCIS codes:** (250.6715) Switching; (130.4815) Optical switching devices; (130.3120) Integrated optics devices

## 1. Introduction

Optical switching technologies can potentially deliver high-bandwidth and modulation-agnostic routing in datacenter networks [1] and enable novel high-performance networking applications such as disaggregated hardware and application-dependent bandwidth allocation [2]. Integrated optical switching devices with radix up to 240×240 has been demonstrated using microelectromechanical systems (MEMS) actuated directional couplers (DC) [3], and Mach-Zehnder interferometer (MZI) based devices have achieved radix up to 64×64 [4]. These large-scale spatial switch fabrics integrate thousands of switching elements (SE) as the fundamental building blocks, which dictate the functionalities and the performance of the fabric.

SE designs can be categorized into two main types: broadband SEs implementing wideband structures such as MZIs [4] and DCs [3], and narrowband SEs implementing wavelength sensitive structures such as microring resonators (MRR) [5]. While broadband SEs can simultaneously route colored wavelength channels, they lack the wavelength selectivity to realize full switching capability in both spatial and wavelength domains, which is desirable to further increase switching granularity for wavelength division multiplexing (WDM) applications [1]. To this end, past demonstrations [6-8] have introduced parallel switching planes implemented with wavelength (de)multiplexers, but the duplication of switching planes poses immense challenges to managing the complexity and footprint of the integrated systems. The work in [9] demonstrated a much miniaturized design by utilizing MRRs as both spatial and spectral filters – multiple MRRs with different resonant wavelengths are coupled to the same bus waveguide, and selectively switch wavelength channels within their respective passbands. The proper operations of MRRs as add-drop filters, however, require careful examination of the critical-coupling conditions, which are susceptible to fabrication variations and environmental drifts.

In this work, we demonstrate a novel space-and-wavelength-selective SE design using MZI assisted by pairs of MRRs. This SE achieves full space and wavelength switching flexibility while remaining miniaturized and robust to design. The MRRs are operated in the over-coupling regime, which significantly improves their tolerance and robustness to fabrication variations. We design, fabricate, and characterize a 2×2×2λ switch block and demonstrate its routing capability in both spatial and wavelength domains within a single MZI structure, introducing a new class of SEs for high-performance space-and-wavelength selective switch fabrics.

## 2. Working Principles and Device Design

Resonator-assisted MZIs have been demonstrated as spatial SEs [10], modulators [11], and wavelength interleavers [12]. Operating in the over-coupling regime, the resonator induces a continuous phase change of $2\pi$ across its resonance. MRR-assisted MZIs leverage slight detuning of a pair of MRRs to induce a large phase difference between the MZI arms. Figs. 1a-1d demonstrate the working principles of an MZI containing one pair of MRRs. By applying a static bias of $\pi/2$ between the two arms, the MRRs can be operated in a push-pull fashion to switch the MZI between its Bar and Cross states. To achieve N-wavelength-selective switching, N pairs of MRRs can be placed along the MZI arms, as illustrated in Fig. 1f. Similar to cascaded add-drop MRRs, the total number of wavelengths supported is limited by the free spectral range (FSR) of the MRRs and each channel's passband. Following these working principles, we design and fabricate a 2×2×2λ SE in a multi-project-wafer (MPW) run through a commercial 200 mm silicon-on-insulator (SOI) platform offered by Advanced Micro Foundry (AMF). Fig. 2a shows the micrograph of the device, integrating 2 multimode interferometers (MMI), 4 MRRs, and 2 MZI thermo-optic (TO) tuners under a footprint of 750 μm×220 μm. MRRs have a racetrack shape with an 8-μm bending radius and a 5-μm straight coupling section. The gap between the MRR and bus waveguide is 100 nm, imposing strong over-coupling conditions. Fig. 2b shows the micrograph of a similar MZI with a single pair of MRRs, which is used to characterize the performance of

the MZI tuner and the MRR phase shifter. For both components, TiN heaters are used to induce localized index change to the silicon waveguides. A folded waveguide design similar to [13] is applied for the MZI tuner to increase phase tuning efficiency while maintain the tuner length under 125 μm.

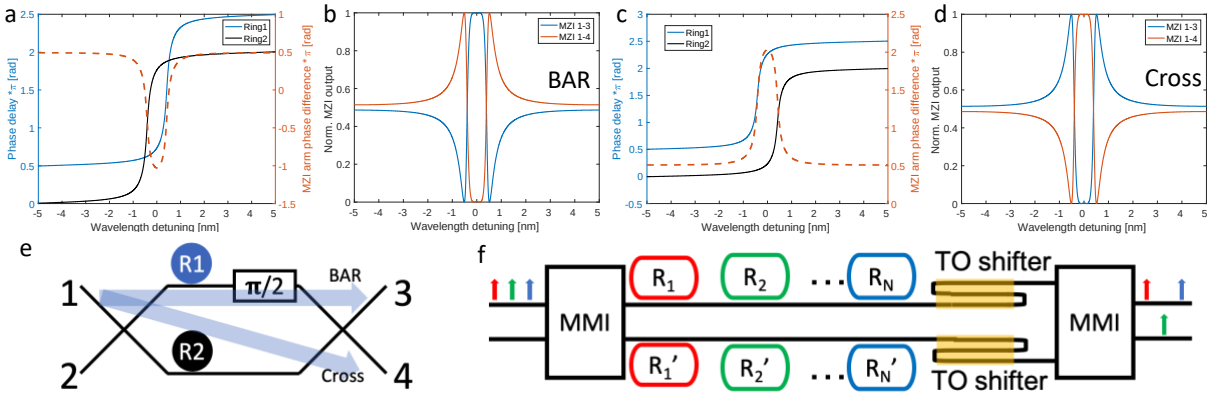


Fig. 1. (a) MRR induced phase difference between MZI arms with static bias of π/2; Ring 1 resonance is red shifted from Ring 2 for Bar state. (b) MZI performs narrowband Bar switching. (c) MRR induced phase difference between MZI arms with static bias of π/2; Ring 1 resonance is blue shifted from Ring 2 for Cross state. (d) MZI performs narrowband Cross switching. (e) Illustration of the Bar and Cross states and MRR indexing. (f) Schematic of multi-wavelength selective switch with MZI assisted by N pairs of MRRs.

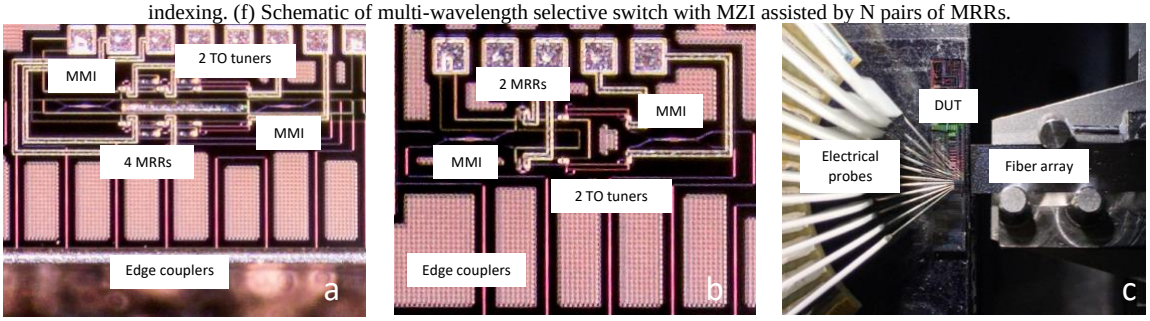


Fig. 2. (a) Micrograph of the 2×2×2λ SE. (b) Micrograph of the SE with a single pair of MRRs. (c) Device under test (DUT) with edge-coupled fiber array and electrical probes.

## 3. Characterization and Analysis

The fabricated devices are accessed optically via edge coupled fiber arrays and electrically via probes, as shown in Fig. 2c. The coupling loss is measured to be ~7 dB per facet with cleaved fiber arrays, which is expected to be largely improved with lensed fibers. As shown in Figs. 3a and 3b, the MZI tuner shows a tuning efficiency of 13.6 mW/π and an MZI extinction ratio (ER) over 32 dB. The MRR shifter shows a tuning efficiency of 0.262 nm/mW and is used to both calibrate the resonance point and perform switching. The spectral profile of the MZI with a single pair of MRRs, whose resonances are far detuned, is shown in Fig. 3c, from which we measure the FSR of the MRRs to be 1.182 THz, and the 3dB-bandwidth to be 101 GHz.

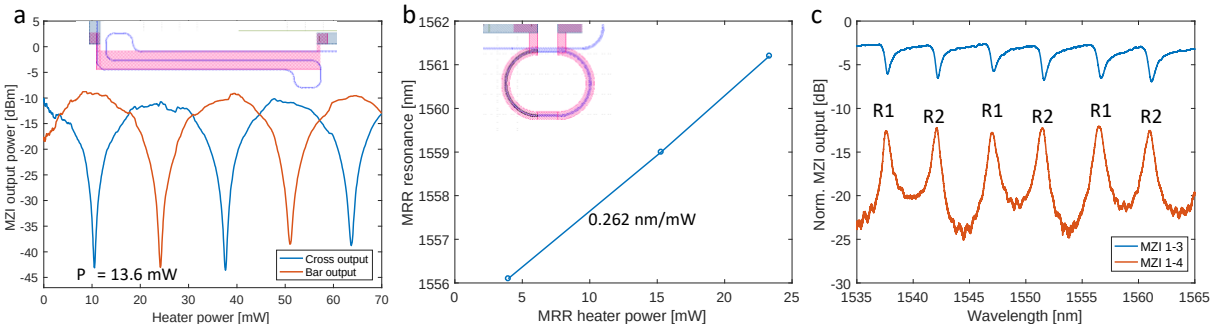


Fig. 3. (a) MZI switching output as a function of TO tuner power consumption. (b) Efficiency of resonance tuning with the TO MRR shifter. (c) Offset MRR resonances while MZI is biased to Bar state, showing clear resonance peaks and FSRs of the MRRs.

For switching characterization, the MZI tuner of the 2×2×2λ SE sets the interferometer at quadrature bias. Two continuous-wave (CW) laser signals, at 1537.3 nm and 1541.3 nm respectively, are combined before inputting to Port 1 of the SE. The resonances of the two pairs of MRRs are set accordingly. In contrast to conventional SE designs with

binary states of Bar and Cross, the WDM-enabled SE supports 4 switching states - (Bar, Bar), (Bar, Cross), (Cross, Bar), and (Cross, Cross), as illustrated in Figs. 4a-4d respectively. Figs. 4e-4h show the SE output spectra for the four switching states. We observe an average crosstalk suppression ratio of 20 dB, as indicated in Figs. 4e-4h. The on-chip loss for switched signal averages to 6.38 dB. By comparing the signal power of a particular channel in an SE state and the leakage power of the same channel in another state, we observe ER of up to 23 dB and 21.8 dB when both channels are assigned to Bar or Cross. In cases when the channels have different states – (Bar, Cross) and (Cross, Bar), the ER is up to 19.2 dB and 19 dB. The modest differences in ER values are attributed to slight thermal crosstalk between the TO shifters. Using a broadband source, we are able to measure the passband spectra of the SE, as shown in Figs. 4i-4l. The Bar state passbands for the two wavelength channels are 112 GHz and 105 GHz, respectively, and the Cross state passbands for the channels are 77 GHz and 70 GHz, respectively.

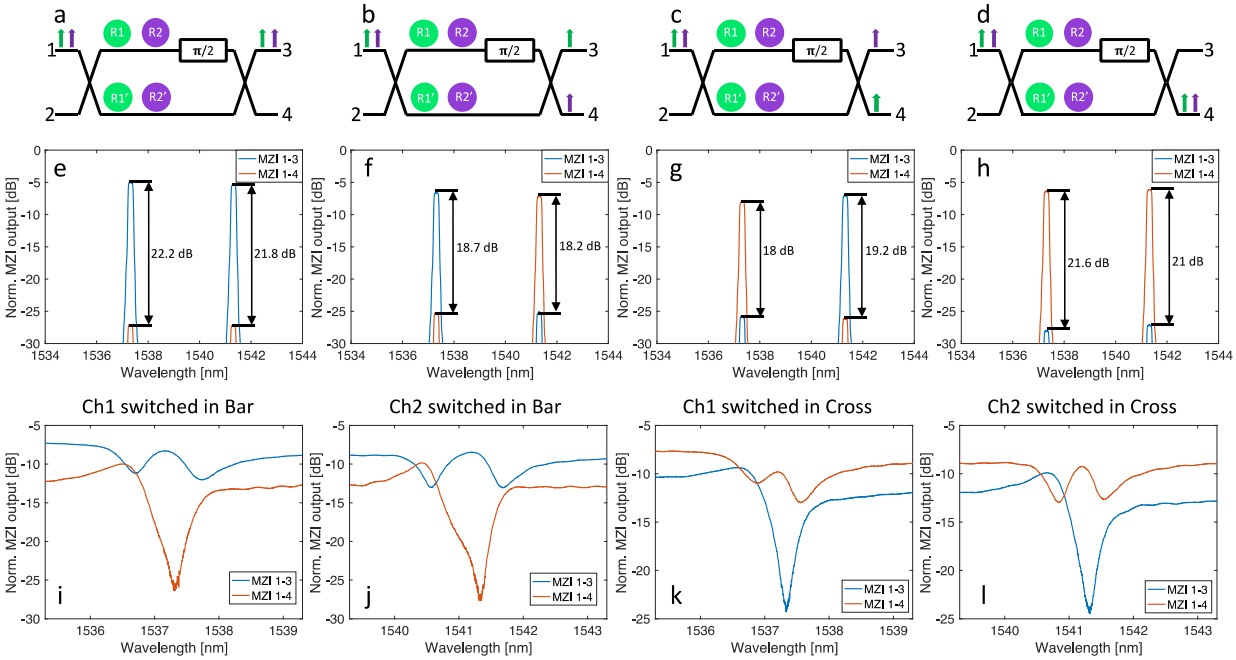


Fig. 4. (a)-(d) Illustrations of (Bar, Bar), (Bar, Cross), (Cross, Bar), and (Cross, Cross) states for two independently switched wavelength channels. (e)-(h) Signal and leakage power levels with two CW lasers in the four switching states. Crosstalk suppression levels are indicated. (i)-(l) Spectra of passband and leakage for both wavelength channels in either Bar or Cross.

## 4. Conclusion

Space-and-wavelength selective switches that allow arbitrary combinations of wavelengths to be selected and routed spatially offer a great flexibility in WDM-based systems. We introduce a novel SE design leveraging an MRR-assisted MZI structure to achieve both spatial and wavelength switching functionalities. The working principles of the design are presented, and we experimentally demonstrate the performance of a 2×2×2λ elementary switch block. The SE switches two wavelength channels independently in a total of four switch states, achieving 20 dB crosstalk suppression and over 19 dB ER. The high performance and compactness of the device make it a promising building block for efficient optical switch fabrics in next generation datacenter networks.

## 5. References


[1] Q. Cheng *et al.*, "Photonic switching in high performance datacenters [Invited]," *Opt. Express*, **26**(12) (2018).
[2] Y. Shen *et al.*, "Silicon photonics for extreme scale systems," *JLT*, **37**(2) (2019).
[3] T. J. Seok et al., "Wafer-scale silicon photonic switches beyond die size limit," *Optica*, **6**(4), (2019).
[4] T. Chu, L. Qiao, W. Tang, D. Guo, and W. Wu, "Fast, high-radix silicon photonic switches," OFC, paper Th1J.4 (2018).
[5] Q. Cheng et al., "Scalable microring-based silicon Clos switch fabric with switch-and-select stages," *JSTQE*, **25**(5), no. 3600111 (2019).
[6] A. Rohit et al., "Monolithic nanosecond-reconfigurable 4×4 space and wavelength selective cross-connect," *JLT*, **30**(17) (2012).
[7] T. J. Seok et al., "MEMS-actuated 8×8 silicon photonic wavelength-selective switches with 8 wavelength channels," CLEO, paper STu4B.1 (2018).
[8] Q. Cheng et al., "Scalable space-and-wavelength selective switch architecture using microring resonators," CLEO, paper STh1N.4 (2019)
[9] A. S. P. Khope et al., "Multi-wavelength selective crossbar switch," *Opt. Express*, **27**(4) (2019).
[10] L. Lu et al., "Low-power 2×2 silicon electro-optic switches based on double-ring assisted Mach–Zehnder interferometers," *OL*, **39**(6) (2014).
[11] C-M. Chang et al., "Differential microring modulators for intensity and phase modulation: theory and experiments," *JLT*, **35**(15) (2017)
[12] L-W. Luo et al., "High bandwidth on-chip silicon photonic interleaver," *Opt. Express*, **18**(22) (2010).
[13] K. Murray et al., "Dense dissimilar waveguide routing for highly efficient thermo-optic switches on silicon," *Opt. Express*, **23**(15) (2015).